ARMY RESEARCH LABORATORY

Design and Response of a Structural Multifunctional Fuel Cell

by Joseph South, Daniel Baechle, Corydon Hilton, Daniel DeSchepper, and Eric Wetzel

ARL-TR-4400   **March 2008**

NOTICES

Disclaimers

The findings in this report are not to be construed as an official Department of the Army position unless so designated by other authorized documents.

Citation of manufacturer's or trade names does not constitute an official endorsement or approval of the use thereof.

Destroy this report when it is no longer needed. Do not return it to the originator.

Army Research Laboratory

Aberdeen Proving Ground, MD 21005-5069

Design and Response of a Structural Multifunctional Fuel Cell

Joseph South, Daniel Baechle, Corydon Hilton, Daniel DeSchepper, and Eric Wetzel
Weapons and Materials Research Directorate, ARL

1. REPORT DATE (DD-MM-YYYY)	2. REPORT TYPE	3. DATES COVERED (From - To)
March 2008	Final	May 2005–October 2005

4. TITLE AND SUBTITLE	5a. CONTRACT NUMBER
Design and Response of a Structural Multifunctional Fuel Cell	5b. GRANT NUMBER
	5c. PROGRAM ELEMENT NUMBER

6. AUTHOR(S)	5d. PROJECT NUMBER
Joseph South, Daniel Baechle, Corydon Hilton, Daniel DeSchepper, and Eric Wetzel	62105AH84
	5e. TASK NUMBER
	5f. WORK UNIT NUMBER

7. PERFORMING ORGANIZATION NAME(S) AND ADDRESS(ES)	8. PERFORMING ORGANIZATION REPORT NUMBER
U.S. Army Research Laboratory ATTN: AMSRD-ARL-WM-MB Aberdeen Proving Ground, MD 21005-5069	ARL-TR-4400

9. SPONSORING/MONITORING AGENCY NAME(S) AND ADDRESS(ES)	10. SPONSOR/MONITOR'S ACRONYM(S)
	11. SPONSOR/MONITOR'S REPORT NUMBER(S)

12. DISTRIBUTION/AVAILABILITY STATEMENT

Approved for public release; distribution is unlimited.

13. SUPPLEMENTARY NOTES

14. ABSTRACT

Many U.S. Army systems, such as ground vehicles and fully equipped Soldiers, are comprised of multiple subcomponents which each typically perform unique functions. Combining these functions into a single, multifunctional component may reduce mass and improve overall system efficiency. Of particular interest are structural materials that also provide power-generating or energy-storing capacity and could provide significant weight savings over a range of platforms. In this study, structural fuel cells are proposed and evaluated. A structural multifunctional fuel cell system is designed so that material elements participating in power and energy processes are also carrying significant structural loads. This synergistic approach allows for mass savings through a multifunctional design. Fabrication and design details for this multifunctional system, as well as structural and power/energy performance results, are reported. Critical material properties and fabrication considerations are highlighted, and important technical challenges are identified.

15. SUBJECT TERMS

fuel cell, composite, multifunctional, power, structural

16. SECURITY CLASSIFICATION OF:			17. LIMITATION OF ABSTRACT	18. NUMBER OF PAGES	19a. NAME OF RESPONSIBLE PERSON Joseph South
a. REPORT	b. ABSTRACT	c. THIS PAGE	UL	34	19b. TELEPHONE NUMBER (Include area code)
UNCLASSIFIED	UNCLASSIFIED	UNCLASSIFIED			(410) 306-0763

Contents

List of Figures

List of Tables

Acknowledgments

INTENTIONALLY LEFT BLANK.

1. Introduction

The performance of many U.S. Army systems depends on the efficient use of material mass and volume. In particular, a large amount of mass and volume in Army systems is dedicated to power generation and energy storage. Energy and power management is a critical aspect of military vehicle design since the duration and intensity of missions are limited by the energy and power density, respectively, available to the vehicle. Therefore, engineers are challenged to increase energy storage and power generation while simultaneously minimizing overall system mass. Examples include next-generation ground vehicles, which will employ hybrid power trains requiring large banks of batteries; unmanned aerial vehicles, whose range and speed are currently limited by battery life; and individual Soldiers, whose sensing and communication equipment requires continuous and burst power requirements. Many of these systems also include significant amounts of structural and/or armor materials. For example, next-generation military ground vehicles are expected to use lightweight metal alloys and polymer composite materials for increased mass efficiency, thereby reducing their logistical footprint.

1.1   Notion of Multifunctional

The conventional approach for improving power and energy density of these military systems is to optimize the performance of individual subcomponents. One set of engineers works to improve the power plant to require less fuel or produce a higher power density. In parallel and independently, materials and structural engineers labor to use novel lightweight materials in structure and armor components, which provide high mechanical efficiency at low weight. The overall system is created by the fastening of the power train to the vehicle structure. Technological advances that allow for a synergistic approach to power and structure can enable higher fuel efficiency, increased range, and a reduced logistical footprint by combining component systems into one multifunctional design (*1–4*). A multifunctional structural fuel cell is a synergistic solution that uses a combined design approach for power generation and structural capability. The objective is to reduce mass overall by designing components that carry loads and participate in power generation or energy storage.

1.2   How Fuel Cells Work

Commercial proton exchange membrane (PEM) fuel cells typically consist of a series-connected stack of individual fuel cells. Each fuel cell contains a membrane electrode assembly (MEA) sandwiched between permeable bipolar plates, such as machined carbon plates, which allow for the circulation of fuel and air sources (*5*). This conventional design is optimized for power, not stiffness or strength. For these traditional fuel cells, power is achieved through appropriate stack design, while the stiffness and strength of the system exist to support the stack and accompanying components.

1.3 The Multifunctional Fuel Cell

In this research, a structural multifunctional fuel cell design is presented so that material elements participating in power or energy processes can also carry significant structural loads. Power and energy components require combinations of materials and components such as dielectrics, electrical conductors, and catalytic or reactive surfaces. Polymer matrix composite (PMC) materials were chosen because they are inherently multi-material systems and are well suited to these complex systems. Secondly, composite material processing provides a great degree of fabrication flexibility. PMC processing requires relatively low temperatures, thus preventing damage to embedded components; it can accommodate complex geometries and subcomponents and is scalable to manufacturing settings.

Figure 1 illustrates the structural fuel cell concept. The design employs a skin-core composite sandwich structure, with thin polymer matrix composite skins and a structural fuel cell core. The structural fuel cell core consists of a conventional MEA between layers of open-cell metallic foam (*6, 7*). The conventional MEA consists of an anode, PEM, cathode and gas diffusion layers. This MEA foam core is contained within thin skins of carbon fiber polymer matrix composite. Aluminum foam was chosen for the core material because it allowed the greatest strength-to-weight ratio. Other metals have been investigated (*8–15*) but not all are available as a foam. The foam geometry was chosen because it provides the shear and compression properties necessary to achieve high structural stiffness, while simultaneously allowing for the circulation of fuel, air, and methanol-water mixture sources to the MEA. Since the metal foam is electrically conductive, it can also simplify component connection by acting as an electron bus between the MEA electrodes and external power wiring.
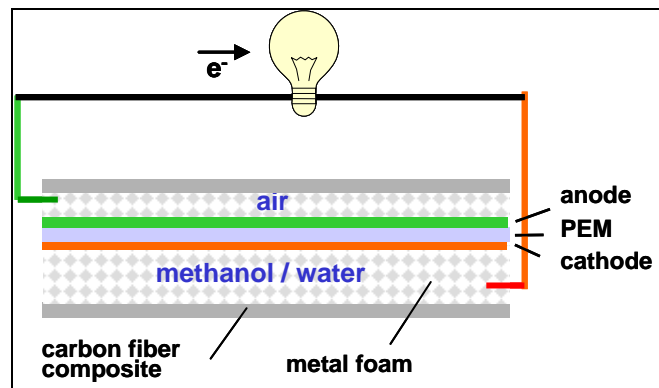
Figure 1. Structural fuel cell concept.

The overall skin-core sandwich structure is a common design approach for creating light structures with high bending stiffness. This stiffness is partly achieved by a core material with a good shear strength. The shear strength of the core allows for load distribution across the sandwich structure. In the case of the multifunction fuel cell, shear strength of the core and the resulting bending stiffness are a challenge because of the presence of the MEA layer along the core shear plane. To investigate this effect, mechanical studies are performed on fuel cell

composites with adhesive layers positioned at various planar positions within the core. Other core mechanical properties can be tailored if the characteristic pore size and wall thickness of the foam core are varied. These foam characteristics also influence flow permeability and electrical contact with the MEA, which could have an effect on power performance.

2. Experimental

The development of a structural multifunctional fuel cell was separated into mechanical performance and power performance investigations. Testing and designs were evaluated separately to identify key parameters that affect each area of performance. The best parameters from each area of investigation were then combined to fabricate a nearly optimized structural multifunctional fuel cell.

2.1 Materials

The multifunctional fuel cell is produced via a single-step composite fabrication technique. The skins of the structure are constructed from unidirectional Bryte Tech AS4 carbon fiber-epoxy pre-impregnated fibers (prepreg). The foam is 6.35-mm-thick aluminum foam from ERG Aerospace, with densities (relative to bulk aluminum) of 6%, 12%, and 20% and pores per inch (ppi) of 10, 20, and 40. Increasing ppi corresponds to a decrease in the characteristic pore size, while increasing density at fixed ppi corresponds to compressing the foam so that the cells begin to collapse onto one another. The foam is adhesively bonded to the skins with an epoxy film adhesive. The MEA is comprised of Nafion[*] 117 sandwiched between layers of carbon cloth with a platinum-ruthinia (Pt/Ru) catalyst layer. The carbon cloth serves as the gas diffusion layer (GDL). The aluminum foam serves as the anode and cathode current collectors.

2.2 Assembly and Processing

Figure 2 shows the layer-by-layer assembly of the basic fuel cell design. All the prepreg plies are overlaid by hand in a continuous 0° or 90° configuration. Four individual ply laminates form the base skin. On top of this skin is a layer comprised of a window of prepreg and an adhesive film. This first prepreg window interior dimensions are sized to match the width and length of the metal foam, and the adhesive film is fabricated to fit into the window. This first prepreg window helps to build up the composite thickness and prevent curvature of the final prepreg skin layers. The metal foam, is placed onto the adhesive and a second prepreg window is placed over the foam. This second prepreg window overlaps the metal foam by 1.26 cm. The MEA completed the sandwich structure and lies directly on the second prepreg window. The entire sandwich is symmetrically constructed about the MEA.

---

[*] Nafion is a registered trademark of E. I. Dupont de Nemours & Co, Inc.
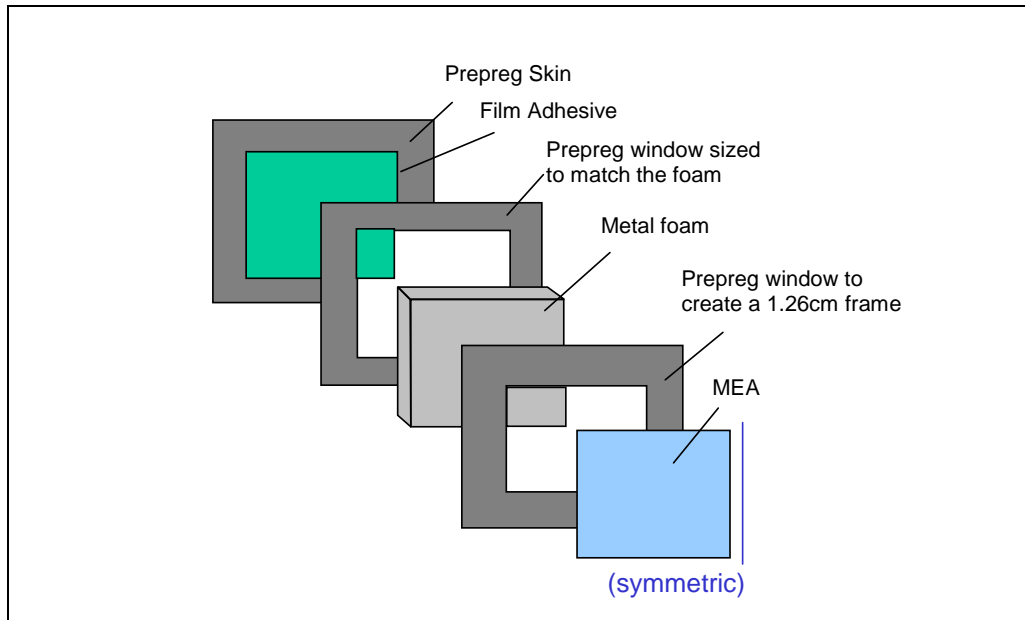
Figure 2. Layer-by-layer assembly of the basic fuel cell design.

The composite is cured under vacuum at 250 °F for 1 hr, which cures both the prepreg and film adhesive layers. The final part has an active MEA area of 10.16 cm. Figure 3 presents a cross section and a top view of the multifunctional fuel cell.
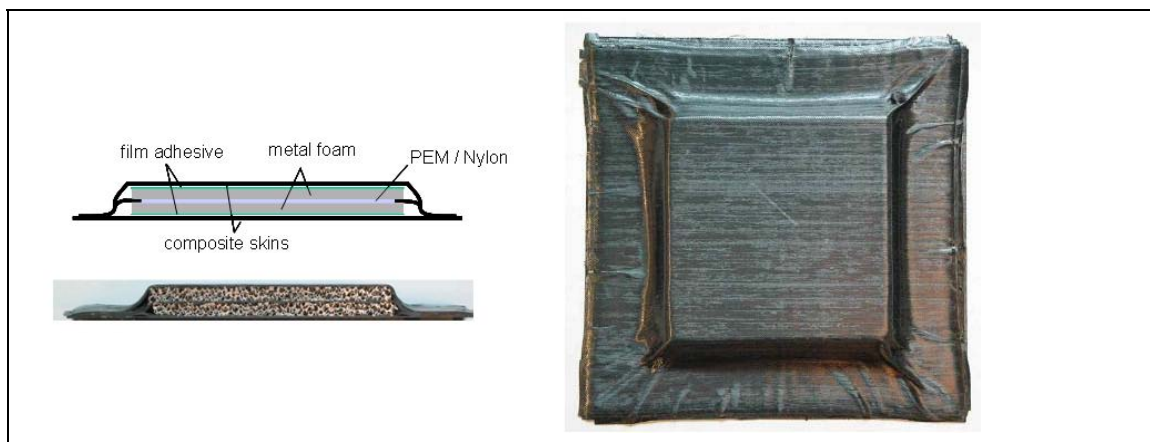
Figure 3. Structural multifunctional fuel cell after fabrication. (The left region is a cross section, while the right portion is a top view.)

2.3   Testing

2.3.1 Mechanical Evaluation and Analysis

We evaluated the mechanical performance by examining eight variables: foam porosity, foam density, location of film adhesive, location of the midplane, incorporation of adhesive strips, integration of an interlocking foam design, and length of the outer skin overlap at the edges of

the cell. These variables and their associated experimental conditions are listed in table 1.
Adhesive layers were situated between the foam cores and the composite skins, and/or at the
midplane between the foam cores. This approach would effectively cut the MEA in half and
would create two fuel cells that are operating with the same anode and cathode. The mechanical
interlock approach was investigated as a means to increase the shear strength of composite. The
combination of interlocking and adhesive strips allows for a potential synergistic effect. The
length of the overlap investigated the effect of the length of composite exposed along the edge of
the fuel cell. The baseline configuration for all of the mechanical testing was 20 ppi, 6% density,
top-bottom adhesive, neutral midplane, no adhesive strips or interlocking foam, and an outer
edge overlap of 12.7 mm.

Table 1. Experimental variables and conditions for the mechanical testing. (The baseline configuration for the
multifunctional fuel cell is shown in italics.)

Variable Name	Condition			
Foam porosity (ppi)	10	*20*	40	—
Foam density (%)	*6*	12	20	—
Location of film adhesive	None	*Top-Bottom*	Middle	All
Location of the midplane	*Neutral*	Lowered 3.175 mm	Raised 3.175 mm	—
Adhesive strips	*None*	Design 1	Design 2	Design 3
Interlocking foam	*None*	Design 1	Design 2	—
Adhesive strips & interlocking	*None*	—	—	—
Length of overlap (mm)	*12.7*	25.4	50.8	—

We conducted mechanical testing of fuel cell cores by sectioning the composite fuel cell into
1.78-cm-wide specimens. Three-point bend experiments were performed at a span of 12.70 cm.
Since the total specimen height of 1.40 cm is higher than allowed under the 16:1 ratio specified
by American Society for Testing Materials D 790-98, results can only be used for comparative
purposes. A total of five measurements was collected for each fuel cell design. To reduce costs
for all mechanical tests, Nylon film was used in place of an actual Nafion MEA layer.

Data from the three-point bend tests were converted to stress and strain figures with the use of
equations from simple beam theory and ASTM C 393 (*16*). Stress in the outer carbon fiber
laminate "skin" at the lengthwise midpoint of each specimen was calculated by the following
equation from ASTM C 393 (*16*):

$$\sigma = \frac{PL}{2t(d+c)b},\qquad(1)$$

where P = applied load (lb), L = support span (in), t = carbon laminate "skin" thickness (in.),
d = total thickness of specimen (in), c = aluminum foam core thickness (in), and b = specimen
width (in). Thicknesses of the carbon fiber laminate skin and the aluminum foam cores were
based on measured averages. Strain in each specimen was calculated by an equation from simple
beam theory, which is also given in ASTM D 790 (*17*). The equation is

$$\varepsilon = \frac{6Dd}{L^2}, \tag{2}$$

where D is the midspan deflection of the beam (in), measured at the crosshead. This equation provides strain in the outer skin of the beam at the lengthwise midpoint of the specimen. Both equations are based on linear elasticity. Data produced with the equations were used to quantify flexural rigidity of each specimen in the linear elastic regime. Outside the region of linear elasticity, the equations are not completely accurate but were still used to qualitatively compare data from different fuel cell designs.

Flexural rigidity values for each specimen were calculated from the slope of the stress-strain plots for strain values between 0.3% and 0.7%. This region was within the linear elastic limits of the specimens. The region of strain before 0.3% was marked by a plateau where stress generally remained constant while strain increased. Thus, this early region could not be included in the rigidity calculation.

Shear stress was also calculated by equation 3 from ASTM C 393 (*16*):

$$\tau = \frac{P}{(d+c)b}. \tag{3}$$

This equation also assumes linear elasticity but can be used to compare the designs outside the elastic region. Shear stress is of particular interest in the aluminum foam and at the midplane of the specimen. The aluminum foam used in the cells had a shear strength of ~1.3 MPa and tensile strength of ~1.2 MPa. Designs with adhesive strips in the midplane help stiffen the fuel cell structure, but the strips can also cause stress concentrations. Shearing of the aluminum foam often started at the edges of adhesive strips in the midplane, leading to failure. These equations have several other limitations. They cannot account for the effects of the length of carbon fiber laminate at either end of the test coupons. The equations cannot account for the different midplane adhesive strip and interlocking designs. However, the changes in stress and strain values caused by these different design parameters are evident in the stress-strain plots and data using these equations.

2.3.2 Power Evaluation

We characterized power performance by evaluating various foam-MEA arrangements in a machined polycarbonate frame. Five layer Generation IV direct methanol fuel cell MEAs were obtained from DuPont. Each MEA possessed a Nafion 117 PEM with a carbon cloth backing with a Pt/Ru anode and a Pt cathode. The minimum metal catalyst concentration was 4 mg/cm^2. The active area for the MEA was 25 cm^2. The aluminum foam was sized to 5×5 cm. Before testing, each MEA was allowed to hydrate for 24 hr in deionized water. The polycarbonate testing frame, figure 4, was sealed with a 4.76-mm-thick foam rubber window piece around the perimeter of the MEA. The two sides of the testing frame were bolted together, thus compressing the foam and sealing the cell. Products and reactants were pumped through

6
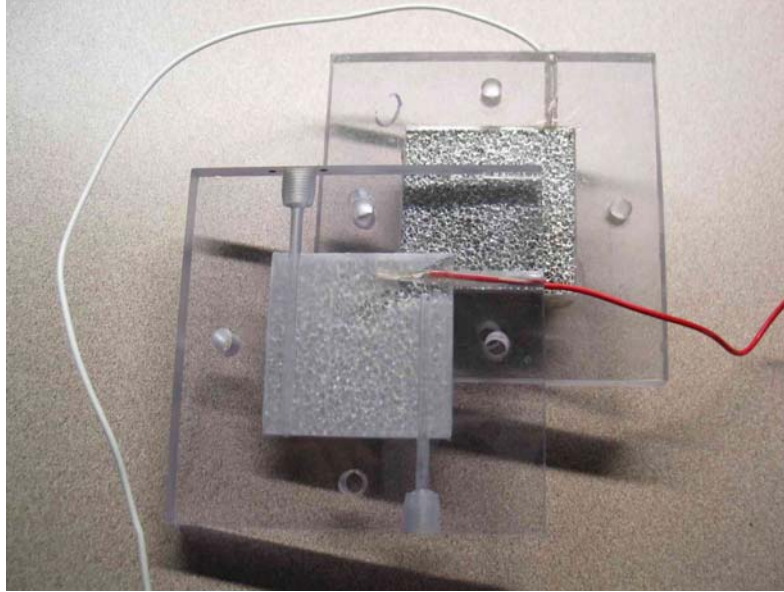
Figure 4. The polycarbonate fuel cell testing frame.

the frame via a peristaltic pump. Electrical connections were made via integrated sealed copper wiring. Testing was conducted via Fuel Cell Technologies' fuel cell testing station connected to the testing frame. We then generated voltage-current (V-I) curves for each test cell by varying the electrical load on the cell while circulating 8 volume-percent aqueous methanol solution in deionized water (2 M methanol) at 207 kPa and 2 cm^3/min and 400 standard cubic centimeters per minute of air at 20 °C. The variables in the power evaluation test are presented in table 2.

Table 2. Experimental variables and conditions for the power performance testing. (The baseline configuration for the multifunctional fuel cell is shown in italics.)

Variable Name	Condition		
Foam porosity (ppi)	10	*20*	40
Foam density (%)	*6*	12	20

3. Results

3.1 Mechanical Performance

The results of the mechanical performance testing of the differing variables and conditions of table 1 are presented in the following sections. We determined the mechanical performance by comparing the average bending stiffness versus the multifunctional fuel cell composite configuration.

3.1.1 Failure Modes

Figure 5 shows a typical loading history. The initial, linear loading portion of the curve is followed by a loss in stiffness and a gradual damage zone under load, eventually leading to sudden failure and a sharp load drop. The bending stiffness of the composite was derived from the elastic portion of the loading curve, as noted in figure 5. Bending stiffnesses of 1 to 10 GPa have been observed.
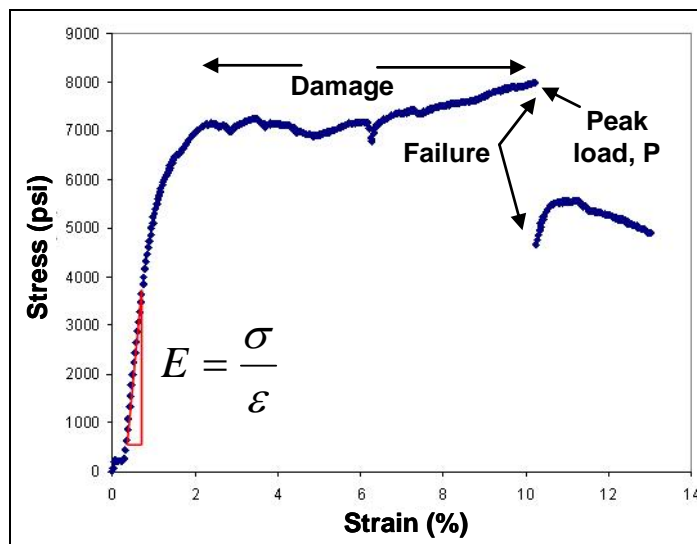
Figure 5. Sample loading history of a structural multifunctional fuel cell.

Damage typically originates as a shear failure at the MEA-foam interface, followed by compressive or shear failure in the foam core, buckling of the composite skins, and eventually composite delamination at the ends of the beam. Typical bending stresses at initial failure are 10 to 50 MPa.

Multiple failure modes were observed during testing. The complexity of the test specimens and the stresses involved in bending tests introduced the possibility of failures in shear, tension, compression, or any combination thereof. Figure 6 presents the five common failure modes for these specimens in bending.

As was mentioned previously, low shear and tensile strength of the aluminum foam, coupled with midplane shear stress concentrations at adhesive strips, led to type 1 failures in the aluminum foam. This failure mode occurred in most samples with adhesive at the midplane. Crushing and buckling of the top carbon fiber laminate skin, or type 2 failure, occurred in almost all samples. This did not always occur at the point of cross-head load application, indicating compressive failure attributable to bending as well as a crushing compressive failure attributable to stress concentration at the point of load application. These same effects caused significant plastic deformation and compressive failure in the aluminum foam immediately under the point

8

Figure 6. Three-point bend specimen observed failure modes.

1 – Aluminum foam shear/tearing
2 – Carbon laminate upper skin compression/buckling
3 – Aluminum foam compression
4 – Delamination at beam end
5 – Midplane shear.

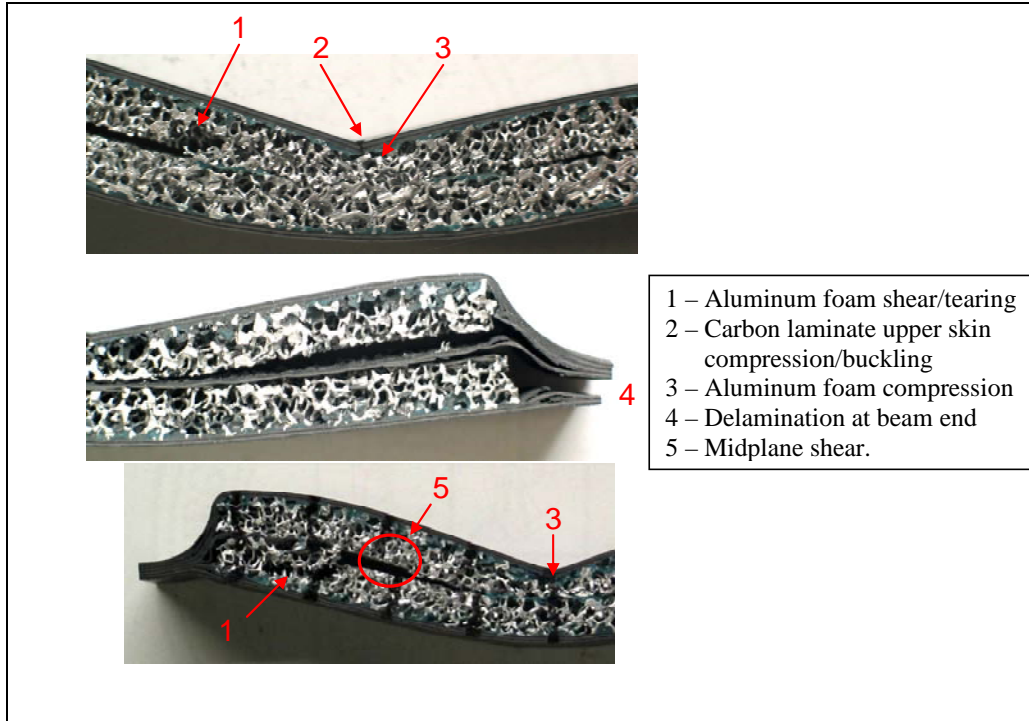of load application (type 3). The length and degree of consolidation of the carbon fiber laminate at either end of the specimen dictated type 4 failure. In some specimens, these "tabs" at either end of the beam extended upward to 2.54 cm beyond the edge of the aluminum foam. Specimens with the longer tabs at either end tended to be stiffer and less likely to delaminate at the ends. However, with proper consolidation of the laminate in these tabs, the problem of delamination could be eliminated in tabs as short as 1.27 cm. While various configurations with adhesive at the midplane did create stiffer and stronger specimens, they were susceptible to type 5 failure: midplane shear. Notice that in figure 6 the black lines in the red circle are not aligned. Before testing, these marks formed a straight line parallel to the axis of load application. Adhesive strips kept the top and bottom pieces of foam from shearing past each other locally, but often, the midplane shear stress caused failure in the adhesive strips or caused the foam near the strips to tear.

3.1.2 Foam Porosity

The effect of aluminum foam porosity on the average bending stiffness is presented in figure 7. The basic design used a 20-ppi foam. Decreasing the porosity to 10 ppi decreased the bending stiffness by 30%. Increasing the porosity to 40 ppi resulted in a small decrease in the bending stiffness; however, this decrease is within the standard deviation of the basic case.
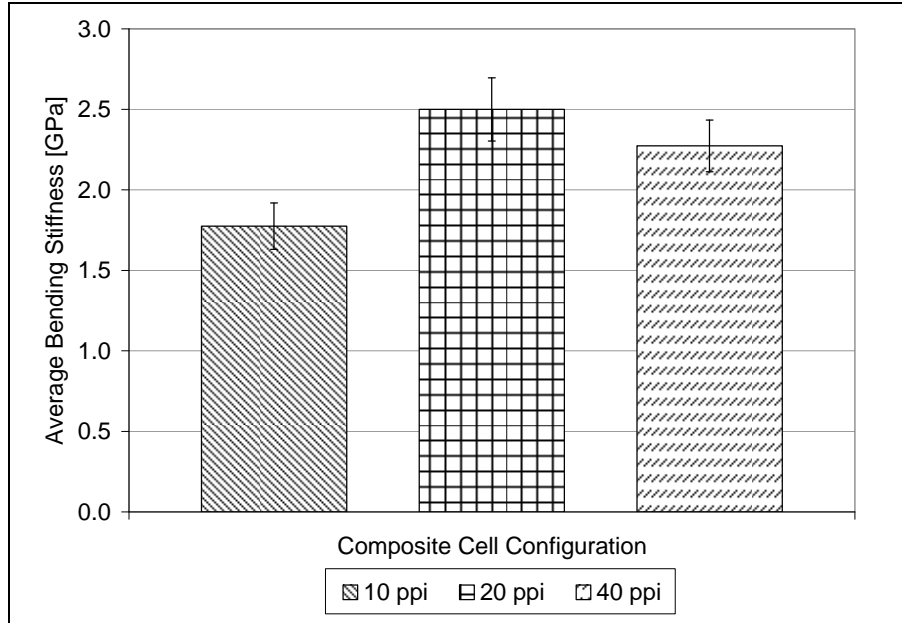
Figure 7. Plot of the average bending stiffness vs. foam porosity.

3.1.3 Foam Density

The effect of the aluminum foam density on the average bending stiffness is presented in figure 8. The basic design used a 6% density foam. The plot shows that an increase in the density of the aluminum foam corresponds to an increase in the average bending stiffness of the overall composite. The increase from 6% to 20% density resulted in a nearly 50% increase in the bending stiffness of the multifunctional fuel cell composite.

3.1.4 Location of the Film Adhesive

The effect of the location of the film adhesive on the average bending stiffness is presented in figure 9. The basic composite design used the film adhesive on the top and bottom. Figure 9 shows a distinctive increase in the average bending stiffness by incorporation of the film adhesive. Inclusion of the adhesive on the top and bottom of the composite doubled the bending stiffness over the no-adhesive case. Incorporation of the adhesive on just the middle layer increased the bending stiffness of the composite by approximately eight times above the no-adhesive case. The use of the adhesive on the top and bottom in conjunction with a midplane adhesive layer resulted in an increase in the bending stiffness an additional 12% over the sole use of the adhesive in the midplane. These data show the importance of shear connectors in the sandwich composite structure. Incorporation of the film adhesive in the midplane effectively creates one continuous piece of aluminum foam and allows the composite to behave more like a traditional skin-core composite.
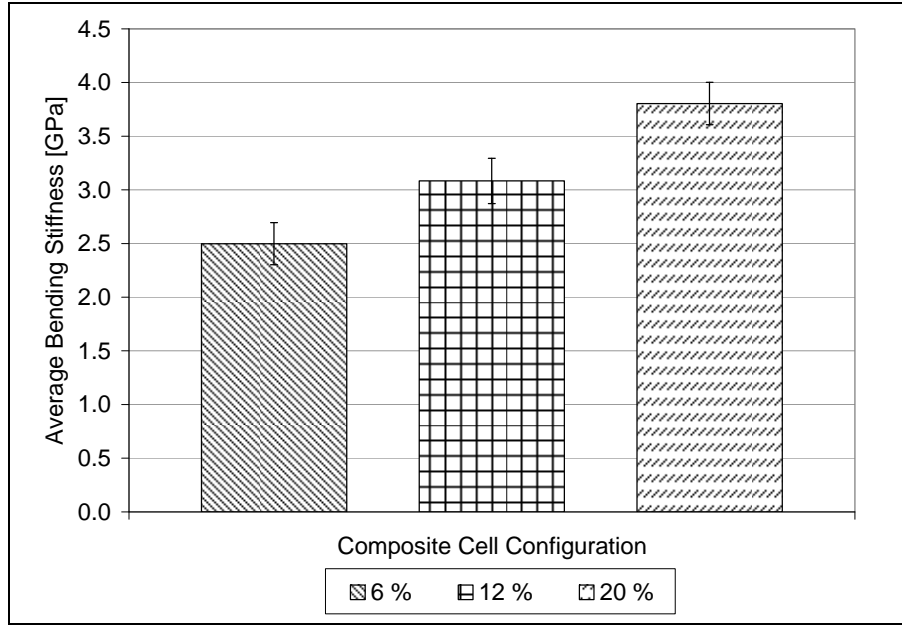
Figure 8. Plot of the average bending stiffness vs. foam density.
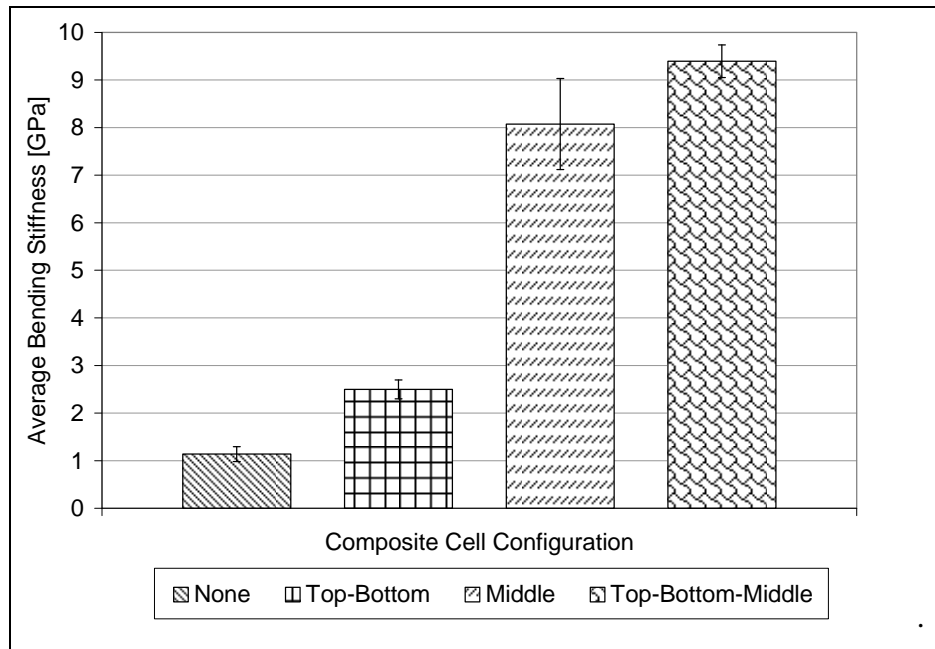
Figure 9. Plot of the average bending stiffness vs. location of the film adhesive.

3.1.5 Location of the Midplane

The effect of the location of the midplane on the average bending stiffness is presented in figure 10. Here, the midplane is defined as the location of the MEA or where the two foam pieces meet. The data in the figure show that there is little difference in changing the location of the midplane of the composite from the neutral location. Lowering the location of the midplane

11
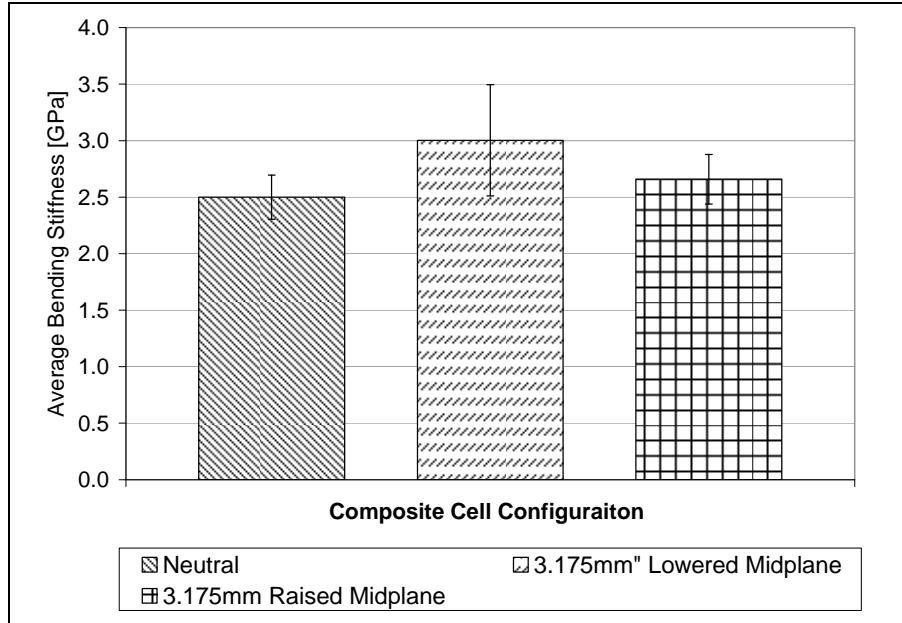
Figure 10. Plot of the average bending stiffness vs. location of the midplane.

by 3.175 mm slightly increases the average bending stiffness; however, this increase is within one standard deviation of the average stiffness for the neutral location. Raising the midplane location by 3.175 mm results in a small increase, but as in the case of lowering the midplane, the average value is within one standard deviation of the neutral location average.

3.1.6 Adhesive Strips

The results of composite cells fabricated with adhesive strips at the midplane are presented in figure 11. The plot shows the effects on the average bending stiffness for three different adhesive strip designs. The designs are presented in table 3.

The result of the adhesive strip design shows that an increase in the average bending stiffness can be obtained. Design 1 had a 12.7-mm strip down the middle of the cell. This design resulted in no appreciable increase over the baseline design. Design 2 increased the width of the adhesive strip by 50%, causing a 200% increase in the bending stiffness. Design 3 split the adhesive strip into two 6.35-mm strips and offset them 25.4 mm from longitudinal midplane of the composite. This design resulted in a 10% stiffness increase over design 2.

3.1.7 Interlocking Foam

The results of composite cells incorporating interlocking foam designs are presented in figure 12. The figure presents the baseline design of no interlocking as well as five interlocking foam variants. Cross sections of the five variants are shown in table 4. The five variants were broken into three different types of designs. Design 2 was a mirror about the midplane of design 1, design 4 was a mirror of design 3, and design 5 was similar to design 4 except that the depth of the interlock was increased. The results of the mechanical testing show a decrease in the average

12
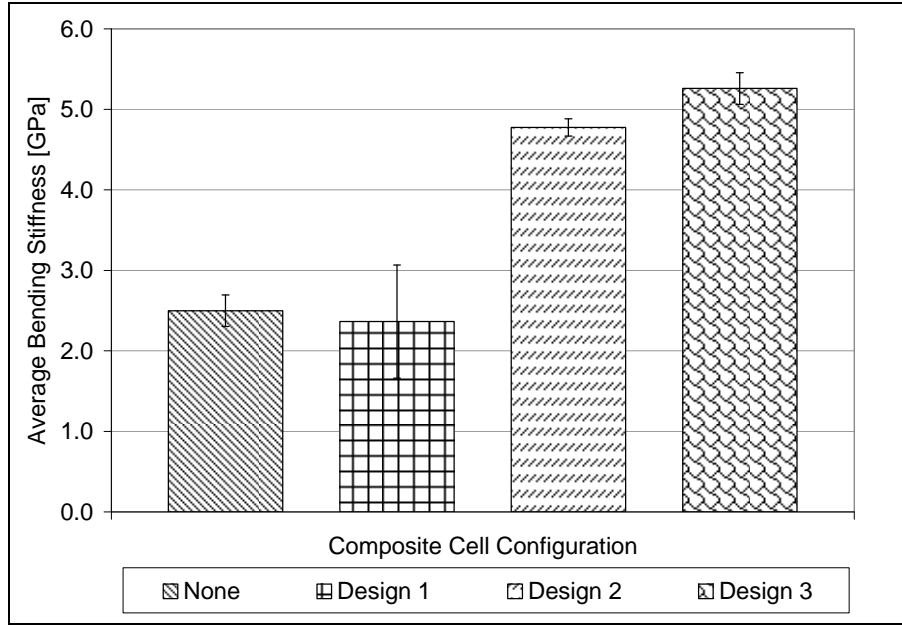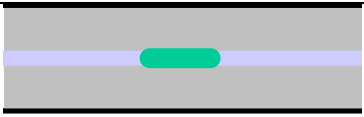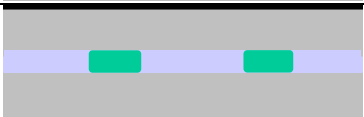
Figure 11. Plot of the average bending stiffness vs. use and location of an adhesive strip.

Table 3. Configuration of the composite cell for the three adhesive strip designs.

Design	Adhesive Configuration	Adhesive Width (mm)	Adhesive Location
1		12.7	Middle
2		19.05	Middle
3		6.35	Offset 25.4 mm from Middle

bending stiffness with the incorporation of the interlocking. In some instances, the stiffness was decreased by more than 60%.

3.1.8 Adhesive Strips and Interlocking Foam

The results of composite cells fabricated with interlocking foam and adhesive strips are presented in figure 13. Interlock design 4, which yielded the lowest stiffness, was combined with adhesive strip designs 2 and 3. The results showed that the combination of interlock design 4 and adhesive strip 2 yielded a decrease in stiffness over the baseline design. The use of the adhesive strip roughly doubled the result of just the interlock alone (figure 12). In the case of interlock design 4 and adhesive strip design 3, the stiffness increased by 75%. This was
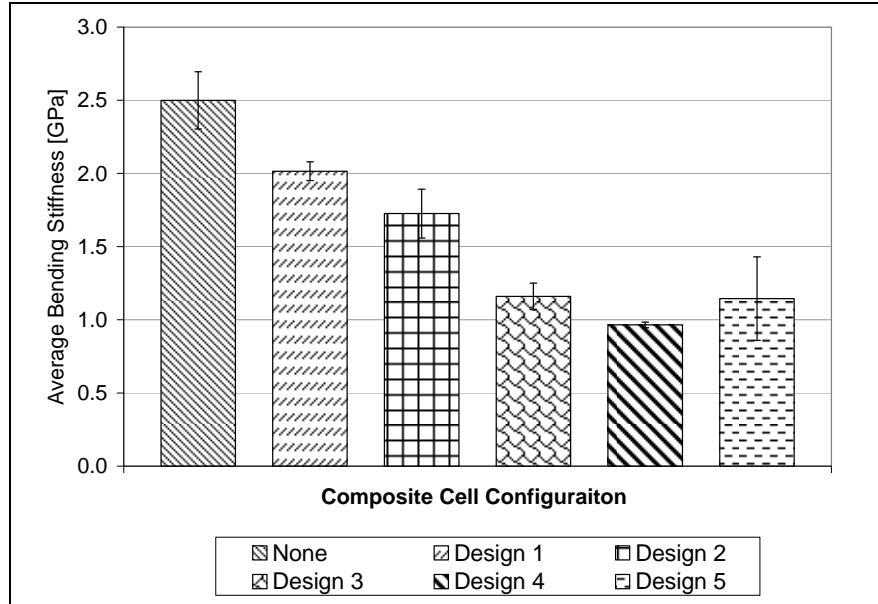
Figure 12. Plot of the average bending stiffness vs. interlocking foam design.

Table 4. Configuration of the composite cell for the five
different interlock configurations.

Design	Interlocking Foam Configuration
1	
2	
3	
4	
5	

nearly a four-fold increase over the interlock design alone. Overall, the use of the adhesive strip
provided an increase over the sole use of the interlock.

3.1.9 Length of Overlap

The results of the length of overlap designs are presented in figure 14. The results show that the
length of the overlap has little to no effect on the average bending stiffness of the composite.
There are slight increases in the bending stiffness with the increase in length to 25.4 and
50.8 mm, but the variation within the results was roughly the same magnitude of the increase.
The stiffness of the multifunction fuel cell design is largely driven by the overall composite lay-
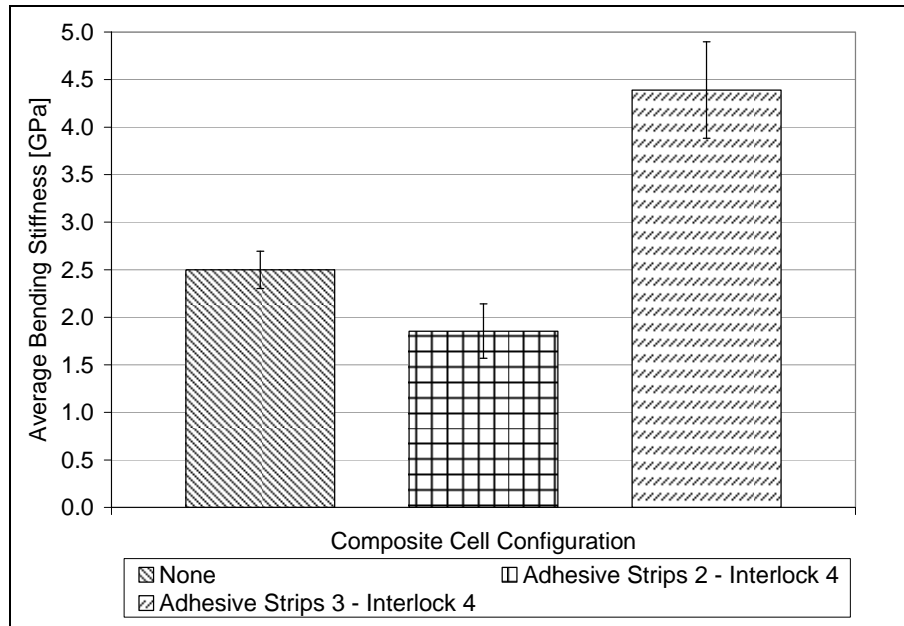up including the use of the adhesive layers.

Figure 13. Plot of the average bending stiffness vs. adhesive strip and interlocking foam design.
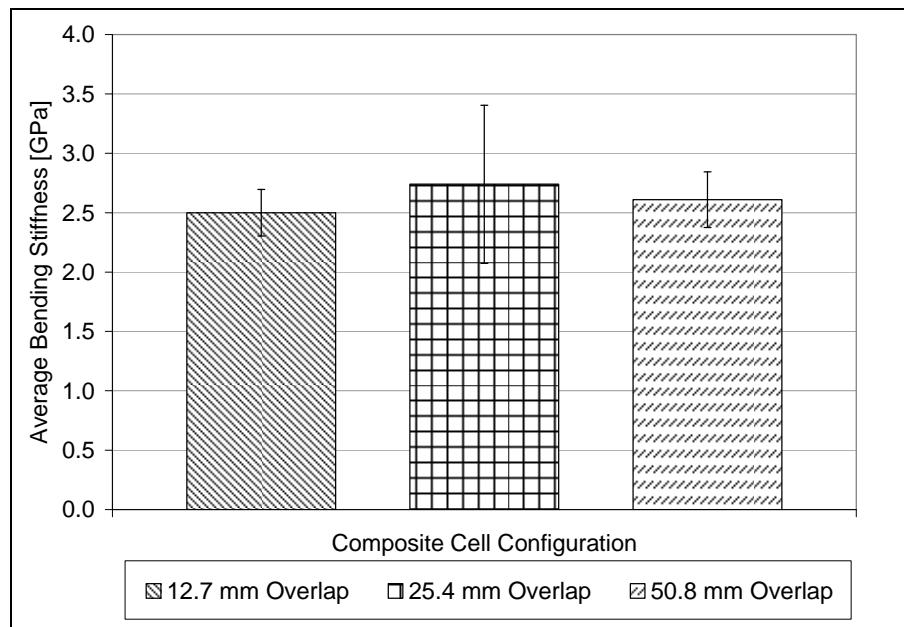
Figure 14. Plot of the average bending stiffness vs. length of overlap design.

3.2 Power Performance

The results of the power performance testing of the different variables and conditions of table 2 are presented in the following sections. We determined the power performance by comparing the polarization and power curves vs. the multifunctional fuel cell composite configuration.

3.2.1 Foam Porosity

The effect of the metallic foam porosity on the power performance of the multifunctional fuel cell is presented in figure 15 which also shows six different curves. The first three curves (open symbols) are the polarization curves for the three difference porosities. The second set of curves (closed symbols) are the power density curves. The power density curves show a clear increase in power density with the increase in the foam porosity. The maximum power density increased by one third when the foam porosity was increased from 10 to 40 ppi. The maximum power density recorded was for the 40-ppi fuel cell at 12.5 mW/cm^2.
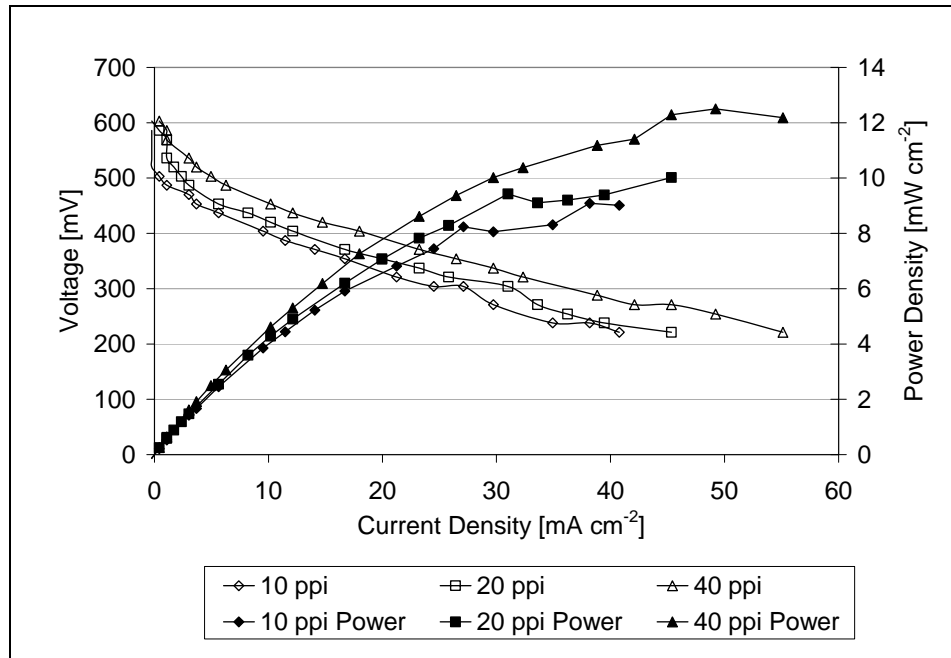
Figure 15. Power performance curves for the three different foam porosities.

3.2.2 Foam Density

Figure 16 presents the power performance curves versus the metallic foam density. The figure shows that there was a clear relationship between foam density and power density. However, unlike the foam porosity, there was not a linear trend. The 12% density fuel cell produced the lowest power density of the three and the 20% density produced the highest power density. The maximum power density recorded was 12.5 mW/cm^2. The 6% density fuel cell was the result and at first tracked well with the 20% results but then fell away at higher current densities.
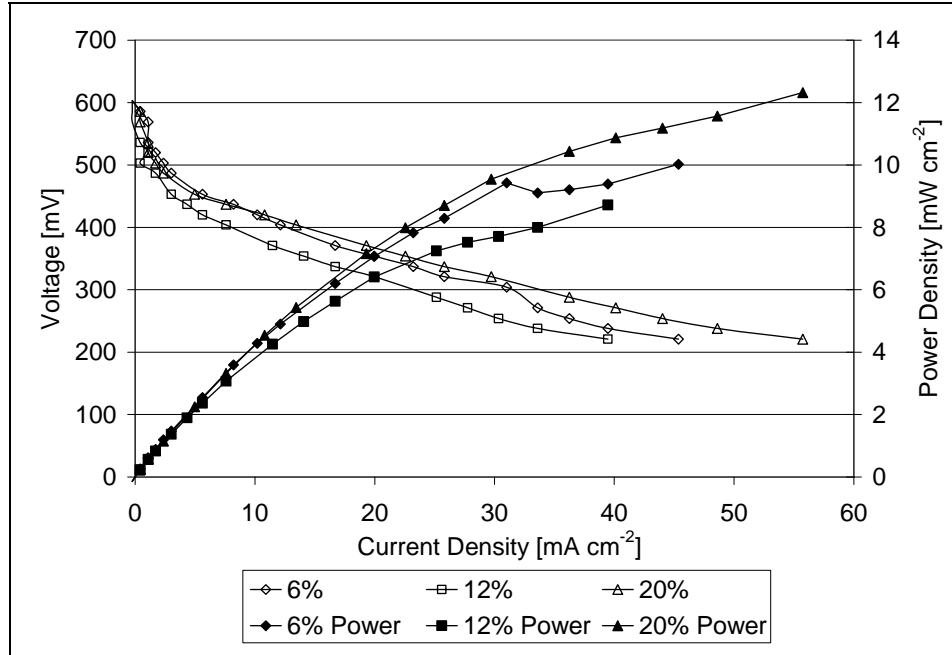
Figure 16. Power performance curves for the three different foam densities.

4. Discussion

The result of the mechanical and power performance testing showed that the stiffness and the power density could be dramatically affected by the component level design of the multifunctional fuel cell.

4.1.1 Mechanical Performance

Bending stiffness generally increased with foam density and porosity. Increased *composite* bending stiffness with increased foam density was likely solely attributable to an increase in *foam* bending stiffness with increasing foam density. Increasing foam porosity from 10 to 20 ppi increased the bending stiffness of the composite. A further increase in porosity to 40 ppi resulted in a decrease in composite bending stiffness, but the 40-ppi sample's stiffness was still higher than that of the 10-ppi sample and was within standard deviation of the 20-ppi sample. Since the density of all three foams was 6%, the pore size decreased as porosity increased. Decreased pore size results in increased number of cell edges and decreased cell edge length, likely creating a stiffer microstructure and overall stiffer foam. However, there could be an optimal porosity for our sample geometry and loading, as evidenced by the decrease in average composite bending stiffness from 20 ppi to 40 ppi.

17

Incorporation of the film adhesive into the component-level design of the multifunctional fuel cell was dramatic. The lowest stiffness was demonstrated with no film adhesive layers, while the highest stiffness was produced by the incorporation of film adhesive at the top, bottom, and midplane of the composite. This design eliminated the shear motion of the foam cores and generated a continuous midplane region, similar to a traditional skin-core composite. Although the maximum bending stiffness was achieved with three adhesive layers, addition of the film adhesive at the midplane alone resulted in a bending stiffness over 300% higher than the basic design with adhesive at the top and bottom of the composite. This increase in bending stiffness shows that the middle adhesive layer dominated composite stiffness by generating a continuous midplane. Although a continuous midplane adhesive layer is not a viable solution for a functional composite fuel cell, these results demonstrate the importance of engineering a fuel cell core with high shear strength.

We examined further effects of midplane shear on the average bending stiffness by shifting the midplane of the composite. Neither raising nor lowering the midplane by 3.175 mm yielded a substantial change in the average bending stiffness. As a result, adhesive strips were examined as a means to reduce the shear between the cores and allow the system to operate as a fully functioning fuel cell. Adhesive strip designs 2 and 3 yielded substantial increases in the average bending stiffness over the basic design. Both designs allowed for the reduction of the relative shear between the foam cores by effectively locking them together. Design 3 used adhesive strips one third the total width of those in design 2, yet resulted in a 10% greater stiffness. This increased stiffness is attributable to the location of the film adhesive away from the central loading axis of the three-point bend test. The strips in design 3 are closer to the ideal location for shear connectors at the midplane, i.e., halfway between the loading point and each support point. The geometry of the three-point bend test dictates the best location of the strips in order to reduce shear motion at the midplane. Thus, tailored usage of the adhesive strips can increase the bending stiffness of the multifunctional fuel cell without completely bonding the middle of the composite together; the latter would prevent the composite from functioning as a fuel cell.

Incorporation of the interlocking foam decreased the average bending stiffness over the baseline design. The original intent of the interlocking was to provide a mechanical interlock that could compensate for the lack of a cohesive midplane. Unfortunately, the relative shearing motion of the midplane and the loss of the structural rigidity of the foam because of the inclusion of the interlocking channels appear to dominate the composite's behavior under load. This loss of stiffness because of the interlocking could be negated through the inclusion of adhesive strips. In fact, the incorporation of the adhesive strip 3 design with the interlock 4 design resulted in a composite bending stiffness more than twice that in the baseline design.

The length of the overlap of the composite at the outer edges was found to have little effect on the average bending stiffness. It is likely that the overlap will contribute to the ultimate bending strength of the composite; however, the bending stiffness appears to be dominated by the shear behavior of the foam cores.

The mechanical performance testing evaluated a series of design variants to determine their effect on the bending stiffness of the multifunctional fuel cell design. These studies demonstrated the importance of shear strength to the design and demonstrated that a modest increase could be obtained if the metallic foam properties were altered. Substantial increases required the addition of an adhesive film to mitigate the midplane shear. Design variants were found that could be used to tailor the bending stiffness of the composite but at the expense of the multifunctional fuel cells' power generation capability.

4.1.2 Power Performance

The power performance testing indicated that power density increased with increases in porosity and density. This trend is similar to that found by Kumar et al. (*6, 7*) and is likely attributed to the decrease in the permeability of the metal foam and an associated uniformity of the local current density. Kumar et al. found that metal foams perform better than conventional channel design flow fields. This performance increase is because as foam permeability decreases, more flow is forced into the GDL which increases reaction rates at the MEA. Our results show that the power density and the polarization curve of the fuel cell can be directly affected if the material properties of the metallic foam are changed.

5. Conclusion

The mechanical and power performance testing showed that the best overall structural multifunctional fuel cell performance would be obtained with foams that have higher porosity or higher density. However, the use of higher density foam may become a limiting factor because of a lower power-to-weight ratio; thus, foams with a higher porosity may be favorable. Optimization of the mechanical performance of a structural multifunctional fuel cell will require the addition of shear connectors at the midplane, preferably through the use of properly placed and sized adhesive strips. Our investigation demonstrates the feasibility of a multifunctional fuel cell; however, continued research efforts are required to combine the mechanical and power-generating capability into a synergistic optimized system. The general conception, design, and implementation of these systems require interdisciplinary coordination and cooperation.

These initial results indicate that multifunctional structural materials, once envisioned, can be realized through the focused development of new materials, material architectures, and fabrication routes.

6. References

1. Thomas, J. P.; Qidwai, M. A. *Acta Materialia*, **2004**, *52*, 2155–2164.

2. Christodoulou, L.; Venables, J. D. Multifunctional Material Systems: The First Generation. *JOM* **2003**, *55*, 39–45.

3. South, J. T.; Carter, R. H.; Snyder, J. F.; Hilton, C. D.; O'Brien, D. J.; Wetzel, E. D. Multifunctional Power-Generating and Energy-Storing Structural Composites for U.S. Army Applications. *Proceedings of the 2004 MRS Fall Conference*, Boston, MA, p 851, 2004.

4. Wetzel, E. D. Reducing Weight: Multifunctional Composites Integrate Power, Communications, and Structure. *AMTIAC Quarterly* **2004**, *8* (4), 91–95.

5. Scott, K.; Taama, W. M.; Argyropoulos, P.; Sundmacher, K. *J of Power Sources* **1999**, *83*, 204–216.

6. Kumar, A.; Reddy, R. G. Materials and Design Development for Bipolar/End Plates in Fuel Cells. *J Power Sources* **2004**, *129*, 62–67.

7. Kumar, A.; Reddy, R. G. Modeling of Polymer Electrolyte Membrane Fuel Cells with Metal Foam in the Flow-Field of the Bipolar/End Plates. *J Power Sources* **2003**, *114*, 54–62.

8. Nikam, V. V.; Reddy, R. G. Corrugated Bipolar Sheets as Fuel Distributors in PEMFC. *International Journal of Hydrogen Energy* **2006**, *31* (13), 1863–1873.

9. Nikam, V. V.; Reddy, R. G. Copper Alloy Bipolar Plates for Polymer Electrolyte Membrane Fuel Cell. *Electrochimica Acta* **2006**, *51*, 6338–6345.

10. Silva, R. F.; Franchi, D.; Leone, A.; Pilloni, L.; Masci, A.; Pozio, A. Surface Conductivity and Stability of Metallic Biploar Plate Materials for Polymer Electrolyte Fuel Cells. *Electrochinica Acta* **2006**, *51,* 3592–3598.

11. Matsuura, T.; Kato, M.; Hori, M. Study of Metallic Bipolar Plate for Proton Exchange Membrane Fuel Cell. *J of Power Sources* **2006**, 123–123.

12. Padhy, B. R.; Reddy, R. G. Performance of DMFC with SS316 Bipolar/End Plates. *J of Power Sources* **2006**, *153*, 125–129.

13. Wind, J.; Spah, R.; Kaiser, W.; Bohm, G. Metallic Biploar Plates for PEM Fuel Cells. *J of Power Sources* **2002**, *105,* 256–260.

14. Makkus, R. C.; Janssen, A. H. H.; de Bruijn, F. A.; Mallant, R. K. A. M. Use of Stainless Steel for Cost Competitive Biploar Plates in the SPFC. *J of Power Sources* **2000**, *86,* 274–282.

15. Weil, K. S.; Kim, J. Y.; Zia, G.; Coleman, J.; Yang, Z. G. Boronization of Nickle and Nickel Clad Materials for Potential Use in Polymer Electrolyte Membrance Fuel Cells. *Surface and Coatings Technology* **2006**, *201* (7), 4436–4441.

16. ASTM C 393. Standard Test Method for Flexural Properties of Sandwich Constructions.

17. ASTM D 790. Standard Test Methods for Flexural Properties of Unreinforced and Reinforced Plastics and Electrical Insulating Materials.

NO. OF
COPIES ORGANIZATION

1   DEFENSE TECHNICAL
(PDF   INFORMATION CTR
ONLY) DTIC OCA
         8725 JOHN J KINGMAN RD
         STE 0944
         FORT BELVOIR VA 22060-6218

1   US ARMY RSRCH DEV &
         ENGRG CMD
         SYSTEMS OF SYSTEMS
         INTEGRATION
         AMSRD SS T
         6000 6TH ST STE 100
         FORT BELVOIR VA 22060-5608

1   DIRECTOR
         US ARMY RESEARCH LAB
         IMNE ALC IMS
         2800 POWDER MILL RD
         ADELPHI MD 20783-1197

1   DIRECTOR
         US ARMY RESEARCH LAB
         AMSRD ARL CI OK TL
         2800 POWDER MILL RD
         ADELPHI MD 20783-1197

1   DIRECTOR
         US ARMY RESEARCH LAB
         AMSRD ARL CI OK T
         2800 POWDER MILL RD
         ADELPHI MD 20783-1197

         ABERDEEN PROVING GROUND

1   DIR USARL
         AMSRD ARL CI OK TP (BLDG 4600)

1	DIRECTOR US ARMY RSRCH LAB AMSRD ARL SE DE R ATKINSON 2800 POWDER MILL RD ADELPHI MD 20783-1197

1	COMMANDER US ARMY MATERIEL CMD AMXMI INT 9301 CHAPEK RD FORT BELVOIR VA 22060-5527

1	OFC OF NAVAL RSRCH J CHRISTODOULOU ONR CODE 332 800 N QUINCY ST ARLINGTON VA 22217-5600

1	NSWC TECH LIBRARY CODE B60 17320 DAHLGREN RD DAHLGREN VA 22448

2	US ARMY RSRCH LAB AMSRD ARL SE DC C LUNDGREN D CHU 2800 POWDER MILL RD ADELPHI MD 20783-1197

1	DIRECTOR US ARMY RESEARCH LAB AMSRD ARL CI J GOWENS BLDG 205 RM 3A012C 2800 POWDER MILL RD ADELPHI M 20783-1197

ABERDEEN PROVING GROUND

1	US ARMY ATC CSTE DTC AT AD I W C FRAZER 400 COLLERAN RD APG MD 21005-5059

12	DIR USARL AMSRD ARL O AP EG FI M ADAMSON AMSRD ARL WM J SMITH

AMSRD ARL WM M
  S MCKNIGHT
AMSRD ARL WM MA
  D DESCHEPPER
  L GHIORSE
  J SNYDER
  M VANLANDINGHAM
  E WETZEL
AMSRD ARL WM MB
  L BURTON
  W DRYSDALE
  M MINNICINO
  J SOUTH

INTENTIONALLY LEFT BLANK.